Journal of Carbon Research

MDPI

Article

MXene@SiC Nanocomposite-Modified Electrode for Sensitive Electrochemical Detection of Cadmium (II) Ions

Diana Konarbay [1], Zhazira Mukatayeva [1,*], Nurgul Shadin [1,*], Yrysgul Bakytkarim [1], Yerbol Tileuberdi [1,2], Nazira Sagatbekova [1], Lishi Wang [3] and Qiang Zeng [3]

[1] Department of Chemistry, Abai Kazakh National Pedagogical University, 13, Dostyk Ave., Almaty 050010, Kazakhstan; konarbay98@bk.ru (D.K.); rysgul_01_88@mail.ru (Y.B.); er.tileuberdi@gmail.com (Y.T.); nazeka.ssss@mail.ru (N.S.)
[2] Abai Green Chemistry Laboratory, Abai Kazakh National Pedagogical University, 30, Kazybek bi st., Almaty 050010, Kazakhstan
[3] School of Chemistry and Chemical Engineering, South China University of Technology, Guangzhou 510640, China; wanglsh@scut.edu.cn (L.W.); ceqzeng@scut.edu.cn (Q.Z.)
* Correspondence: zh.mukatayeva@abaiuniversity.edu.kz (Z.M.); nugen_87@mail.ru (N.S.); Tel.: +7-707-706-77-98 (N.S.)

Abstract

Cadmium (II) ions are highly toxic contaminants that can pose significant risks to environmental and human health, necessitating the development of sensitive and reliable analytical methods for their determination. In this study, an MXene@SiC nanocomposite-modified glassy carbon electrode (MXene@SiC/GCE) was developed for the electrochemical detection of Cd (II) ions. Carbon-based materials have been widely investigated for electrochemical sensing due to their high electrical conductivity, large specific surface area, and properties that enhance electron transfer. The MXene@SiC nanocomposite was prepared by combining $Ti_3C_2T_x$ MXene and SiC at a 1:1 mass ratio. The structural and surface characteristics of the prepared materials were investigated by SEM, EDS, and FTIR analyses, confirming the successful integration of MXene and SiC. The electrochemical properties of the modified electrode were evaluated by cyclic voltammetry using the $[Fe(CN)_6]^{3-}/[Fe(CN)_6]^{4-}$ redox probe. The effect of key experimental parameters, including scan rate, pH, accumulation time, and deposition potential, was investigated. The optimum conditions were found to be pH 5, an accumulation time of 350 s, and a deposition potential of −1.2 V. Under optimized conditions, the MXene@SiC/GCE exhibited a well-defined Cd(II) stripping response at approximately −0.9 V. Two linear concentration ranges were obtained: 0.5–1000 µg/L with the calibration equation $I = 0.2932C + 1.5916$ ($R^2 = 0.9893$) and a higher concentration range with $I = 0.04911C + 33.6442$ ($R^2 = 0.9643$). The developed electrode demonstrated a concentration-dependent response and satisfactory electrochemical characteristics, indicating that the MXene@SiC nanocomposite is a promising electrode-modifying material for Cd(II) determination in aqueous samples.

Keywords: MXene@SiC; $Ti_3C_2T_x$ MXene; silicon carbide; Cd(II); electrochemical sensor; differential pulse voltammetry; glassy carbon electrode; heavy metal detection

Check for updates

Academic Editor: Sergey Mikhalovsky

Received: 1 October 2026
Revised: 1 November 2026
Accepted: 12 November 2026
Published: 19 November 2026

Copyright: © 2026 by the authors. Licensee MDPI, Basel, Switzerland. This article is an open access article distributed under the terms and conditions of the Creative Commons Attribution (CC BY) license.

1. Introduction

Cadmium (Cd^{2+}) is a non-essential heavy metal characterized by high toxicity, environmental persistence, and the ability to accumulate in living organisms, posing a significant threat to human health and ecosystems. The rapid development of industrial sectors such as mining, electroplating, battery and pigment production, metallurgy, and phosphate

fertilizer manufacturing has contributed to the release of large amounts of cadmium into the environment, resulting in increased concentrations in aquatic ecosystems. Unlike many organic pollutants, cadmium does not degrade under natural conditions and remains in soil and water for long periods. Once released into the environment, Cd^{2+} accumulates in plants, aquatic organisms, and throughout the food chain, posing a serious threat to ecosystems and human health. Long-term exposure to cadmium may cause kidney dysfunction, bone demineralization, damage to the nervous system, cardiovascular diseases, and the development of cancer. Therefore, continuous monitoring of trace levels of Cd^{2+} ions in environmental and food samples has become one of the important tasks for ensuring environmental safety and protecting public health [1–3].

High-precision instrumental techniques such as atomic absorption spectrometry (AAS), inductively coupled plasma optical emission spectrometry (ICP-OES), inductively coupled plasma mass spectrometry (ICP-MS), and X-ray fluorescence (XRF) analysis are widely used for the quantitative determination of Cd^{2+} ions. These methods provide high sensitivity, low detection limits, and accurate analytical results. However, their application requires expensive instrumentation, complicated sample preparation, specialized laboratory facilities, and the involvement of qualified personnel. These limitations prevent their widespread application for rapid on-site analysis and real-time monitoring. Therefore, the development of simple, portable, highly sensitive, and cost-effective analytical platforms for Cd^{2+} ion detection has become one of the major research directions in modern electroanalytical chemistry [4–7].

Electrochemical sensors are considered one of the most promising analytical approaches for the detection of heavy metal ions owing to their high sensitivity, rapid analysis, ease of operation, relatively low cost, and compatibility with portable devices. Among these methods, anodic stripping voltammetry (ASV), particularly differential pulse anodic stripping voltammetry (DPASV) and square-wave anodic stripping voltammetry (SWASV), is widely used for the determination of trace concentrations of heavy metal ions such as Cd^{2+} because of its effective preconcentration step and its ability to achieve low detection limits. Furthermore, the analytical performance of electrochemical sensors is mainly determined by the physicochemical properties of the electrode material. Therefore, considerable attention has been devoted in recent years to the development of novel functional electrode materials with high electrical conductivity, a large specific surface area, abundant active sites, and rapid electron transfer capability [8–12].

The rapid development of nanotechnology has enabled the widespread application of functional nanomaterials in the fabrication of next-generation electrochemical sensors. At present, carbon nanomaterials, metal nanoparticles, conductive polymers, metal–organic frameworks (MOFs), and two-dimensional (2D) materials are being extensively investigated to improve the sensitivity, selectivity, and stability of electrochemical sensors. Among these materials, two-dimensional nanostructures have attracted particular attention because of their large specific surface area, high electrical conductivity, and abundance of active sites. These characteristics facilitate electron transfer at the electrode/electrolyte interface, enhance the efficiency of electrochemical reactions, and improve the analytical performance of electrochemical sensors [13]. Carbon-based materials have attracted considerable attention in electrochemical sensing because of their high electrical conductivity, large surface area, and tunable surface properties. Recent studies have demonstrated that carbon-derived materials, including coke-derived carbon, can be effectively combined with silicon carbide to construct nanocomposite electrodes for sensitive heavy metal detection. In addition, multi-walled carbon nanotubes have been integrated with gold nanoparticles on glassy carbon electrodes, where their large surface area and conductivity, together with the enhanced electron-transfer and adsorption properties of gold nanoparticles, contributed to

improved sensing performance. Carbon-based sensing platforms have also been extensively investigated for the electrochemical determination of toxic heavy metal ions such as Pb^{2+}, Cd^{2+}, and Hg^{2+}, highlighting their potential for environmental water monitoring. These findings demonstrate that combining carbon-based materials with complementary functional components is an effective strategy for improving electrode surface properties and electrochemical sensing performance [14–17].

Since their first synthesis through the selective etching of MAX phases, MXene materials have become one of the most promising two-dimensional nanomaterials for electrochemical applications [18,19]. Among the MXene family, $Ti_3C_2T_x$ is distinguished by its high electrical conductivity, hydrophilic surface, abundance of -O, -OH, and -F functional groups, as well as its large specific surface area. These structural characteristics facilitate efficient electron transfer, enhance the adsorption of target analytes onto the electrode surface, and increase the number of electrochemically active sites. As a result of these advantages, $Ti_3C_2T_x$ MXene has been widely applied in energy storage systems, electrocatalysis, biosensors, and the development of electrochemical sensors for environmental monitoring [20–23].

Numerous studies have demonstrated that MXene-based electrodes exhibit high electrochemical activity for the detection of heavy metal ions. For example, alkalized Ti_3C_2 MXene has been successfully used for the simultaneous determination of Cd(II), Pb(II), Cu(II), and Hg(II) ions. In addition, it has been reported that combining MXene materials with metal oxides, metal–organic frameworks, carbon nanotubes, or graphene derivatives significantly improves the sensitivity and selectivity of electrochemical sensors [24,25]. Nevertheless, pristine MXene possesses certain inherent limitations. Strong van der Waals interactions between adjacent layers lead to the restacking of MXene nanosheets, thereby reducing the active surface area and decreasing the number of electrochemically active sites. Furthermore, MXene is gradually oxidized under ambient conditions, which may result in a decline in its electrical conductivity and long-term stability [24,25].

One of the most effective approaches to overcome the aforementioned limitations of MXene materials is the construction of MXene-based hybrid nanocomposites. The incorporation of additional functional components prevents the restacking of MXene layers, improves the structural stability of the material, increases the number of active sites, and promotes faster electron transfer. As a result of this synergistic effect, hybrid nanocomposites exhibit higher electrochemical activity, improved charge-transfer properties, and superior analytical performance compared with pristine MXene materials [26–31].

Among semiconductor materials, silicon carbide (SiC) is distinguished by its chemical inertness, corrosion resistance, excellent mechanical strength, high thermal conductivity, and favorable electrical properties. In particular, porous and nanostructured SiC possesses a large specific surface area and a well-developed surface structure, which enhance electrochemical processes and facilitate charge transfer. Owing to these advantages, SiC has been widely investigated and applied in the development of various functional materials, including photodetectors, catalytic systems, energy storage devices, and electrochemical sensors [32–34].

From a materials science perspective, integrating $Ti_3C_2T_x$ MXene and SiC into a single nanocomposite enables the complementary combination of their individual advantages and promotes the formation of a synergistic effect. The high electrical conductivity of MXene provides efficient electron transport, whereas SiC particles suppress the restacking of MXene layers, preserve the structural stability of the composite, and contribute to increasing the number of accessible electrochemically active sites. Such a hybrid structure accelerates charge-transfer kinetics and enhances the adsorption of Cd(II) ions onto the electrode surface, thereby improving the sensitivity, electron-transfer rate, and overall analytical performance of the sensor [35,36]. Although MXene -based composite materials have been

extensively investigated in the field of electrochemical sensing, studies on MXene@SiC hybrid systems for the detection of Cd(II) ions remain limited. Therefore, the development of MXene@SiC-modified electrodes with improved structural stability, high sensitivity, and enhanced electrochemical performance is of considerable scientific interest and practical significance for the rapid and accurate determination of cadmium ions in environmental samples [37]. The proposed strategy for the fabrication of the MXene@SiC nanocomposite and its application for electrochemical Cd(II) detection is schematically illustrated in Figure 1. In Figure 1, the black and blue curves represent the DPV responses of Cd(II) ions obtained using the bare GCE and MXene@SiC-modified GCE, respectively.

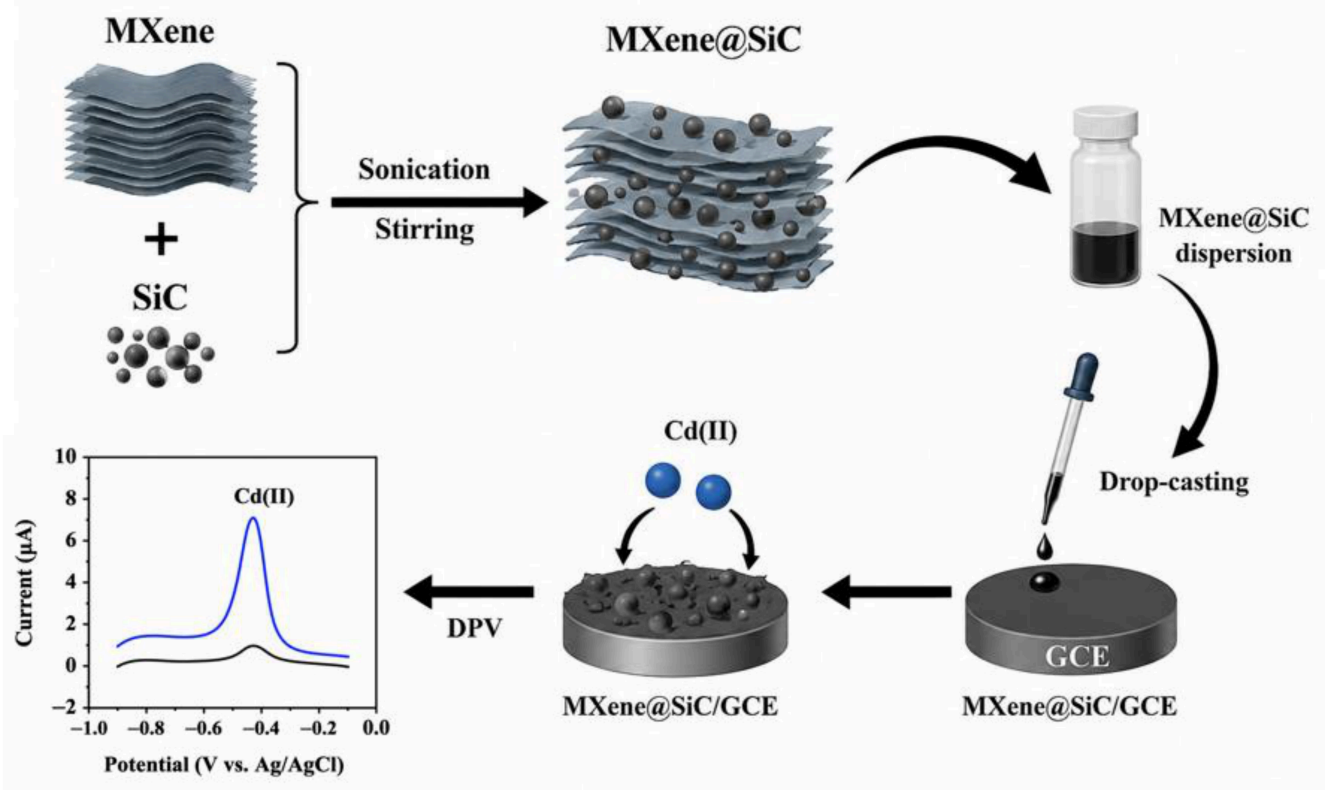


Figure 1. Schematic illustration of MXene@SiC nanocomposite preparation and its application for electrochemical detection of Cd(II) ions.

In this work, a glassy carbon electrode modified with an MXene@SiC nanocomposite was fabricated for the highly sensitive detection of Cd(II) ions, and its potential application as an electrochemical sensor was investigated. The structural and morphological characteristics of the synthesized nanocomposite were comprehensively characterized, while its electrochemical behavior was evaluated using cyclic voltammetry (CV), electrochemical impedance spectroscopy (EIS), and differential pulse voltammetry (DPV). Furthermore, the analytical performance of the fabricated sensor, including its sensitivity, linear working range, limit of detection, repeatability, and selectivity, was systematically evaluated. The obtained results demonstrated that the combination of MXene and SiC produced a pronounced synergistic effect and confirmed that the MXene@SiC nanocomposite is a promising electrode material for the reliable and efficient determination of Cd(II) ions at low concentrations. A schematic representation of the MXene@SiC-modified glassy carbon electrode and the subsequent electrochemical detection of Cd(II) ions is presented in Figure 2. In Figure 2, curves a and b represent the DPV responses of Cd(II) ions obtained using the bare GCE and MXene@SiC-modified GCE, respectively.

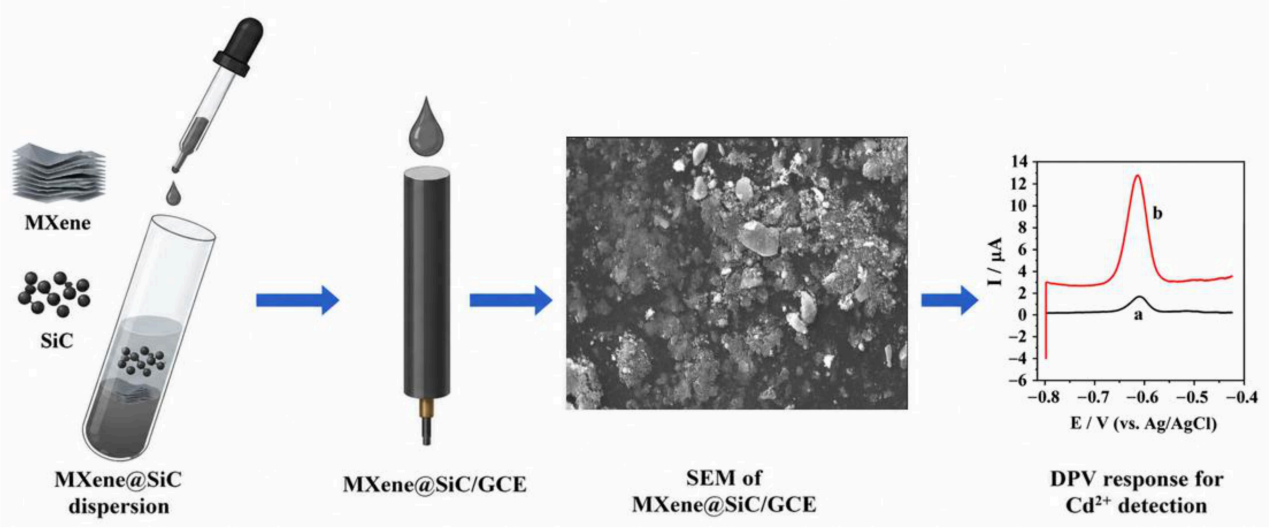


Figure 2. Schematic illustration of MXene@SiC-modified glassy carbon electrode fabrication and electrochemical detection of Cd(II) ions.

The electrochemical behavior of Ti_3C_2 MXene-based electrodes in heavy metal ion detection has also been reported in previous studies. In particular, Qian et al. [38] demonstrated the application of an alkalized Ti_3C_2 MXene-modified pencil graphite electrode for the simultaneous electrochemical detection of Cd(II) and Pb(II), highlighting the potential of MXene-based materials for heavy metal sensing.

This schematic illustrates the overall experimental strategy, from the preparation of the MXene@SiC nanocomposite and modification of the glassy carbon electrode to the subsequent electrochemical detection of Cd(II) ions.

2. Results and Discussion

2.1. Surface Morphology

The morphology of MXene, SiC, and the MXene@SiC nanocomposite was investigated using scanning electron microscopy (SEM), as shown in Figure 3. The MXene material (Figure 3A,B) is characterized by a typical layered and accordion-like structure. At lower magnification (Figure 3A), the material consists of irregularly stacked and partially separated flakes with clearly visible interlayer spaces. In some regions, the sheets are closely stacked on top of one another, whereas in other areas, the layers are randomly oriented and partially delaminated. At higher magnification (Figure 3B), the multilayered architecture becomes more pronounced, with individual lamellar sheets and expanded interlayer regions clearly visible. The observed morphology is characteristic of a layered MXene structure and provides accessible channels for electrolyte penetration and ion transport.

The morphology of the synthesized SiC is shown in Figure 3C,D. At lower magnification (Figure 3D), SiC exhibits a heterogeneous surface consisting of numerous irregularly distributed granular regions and agglomerated structures. The particles tend to form clusters of different sizes, indicating a pronounced tendency toward aggregation. At higher magnification (Figure 3C), the surface of the SiC aggregates appears rough and non-uniform, consisting of densely packed fine particles and irregular structural features. The apparent dimensions of the larger SiC aggregates observed in the SEM image range approximately from 1.0 to 3.8 μm. These dimensions correspond to aggregated regions rather than individual SiC nanoparticles. The observed agglomeration may be attributed to strong interparticle interactions and the high surface energy of the SiC particles.

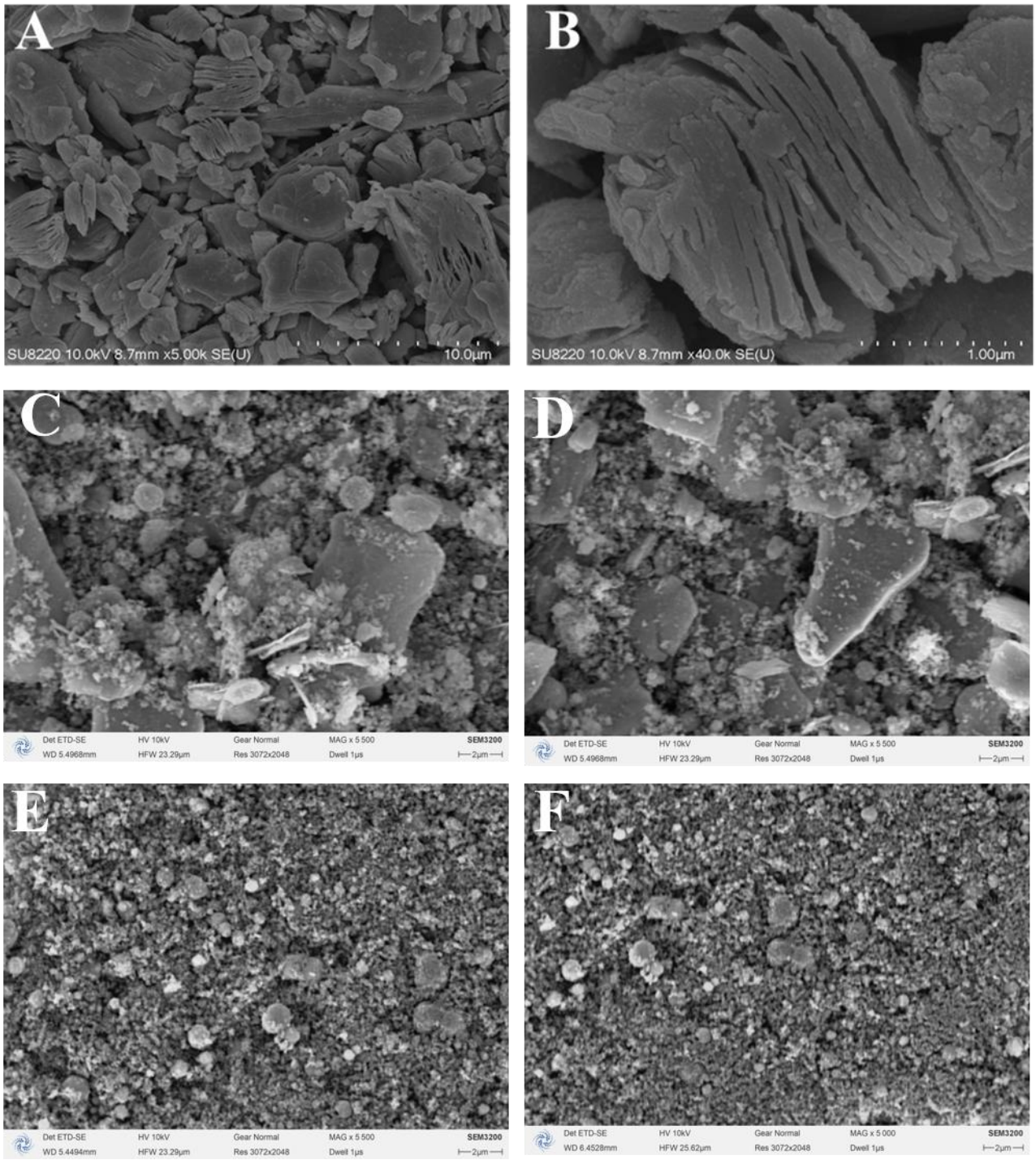


Figure 3. SEM images of (**A**,**B**) MXene, (**C**,**D**) SiC, and (**E**,**F**) MXene@SiC nanocomposite.

To evaluate the morphological changes resulting from the integration of SiC with MXene, the MXene@SiC nanocomposite was further examined by SEM, as shown in Figure 3E,F. At lower magnification (Figure 3F), the composite exhibits a heterogeneous and relatively rough surface consisting of a continuous matrix decorated with irregularly shaped granular and larger particulate structures. Compared with pristine MXene, the surface morphology becomes substantially more heterogeneous after incorporation of SiC. At higher magnification (Figure 3E), numerous fine granular features and irregularly shaped agglomerates are observed throughout the matrix. The apparent dimensions of the larger structures range

approximately from 1.2 to 6.8 μm. These features are considered to represent aggregated regions rather than individual SiC nanoparticles.

The comparison of the three materials reveals a clear morphological evolution from the layered structure of MXene and the granular, agglomerated morphology of SiC to the more complex hybrid architecture of the MXene@SiC nanocomposite. In the composite, the SiC-containing structures are distributed across the MXene-based matrix, while the layered features of MXene remain partially distinguishable. This morphology indicates close interfacial contact between the two components and suggests the formation of an integrated hybrid structure. The combination of the conductive layered MXene framework with the rough and heterogeneous SiC phase may increase the accessible surface area and provide additional interfacial sites.

Such a morphology is favorable for electrochemical applications because the layered MXene structure can facilitate electron transport, while the rough SiC-containing domains can contribute additional surface sites for interaction with the electrolyte. The heterogeneous and interconnected surface of the MXene@SiC nanocomposite may also promote electrolyte penetration and improve the accessibility of Cd^{2+} ions to the electrode interface. Therefore, the observed morphology is expected to facilitate interfacial charge transfer and the accumulation of Cd^{2+} ions, contributing to the enhanced electrochemical performance of the MXene@SiC-modified electrode.

2.2. Elemental Characterization of the MXene@SiC Nanocomposite

The elemental composition of the synthesized MXene@SiC nanocomposite was examined by energy-dispersive X-ray spectroscopy (EDS). As shown in Figure 4, the EDS spectrum confirms the presence of C, O, F, Si, Al, and Ti in the analyzed material. The quantitative analysis gives weight fractions of 24.49% C, 9.11% O, 1.70% F, 46.91% Si, 0.25% Al, and 17.54% Ti.

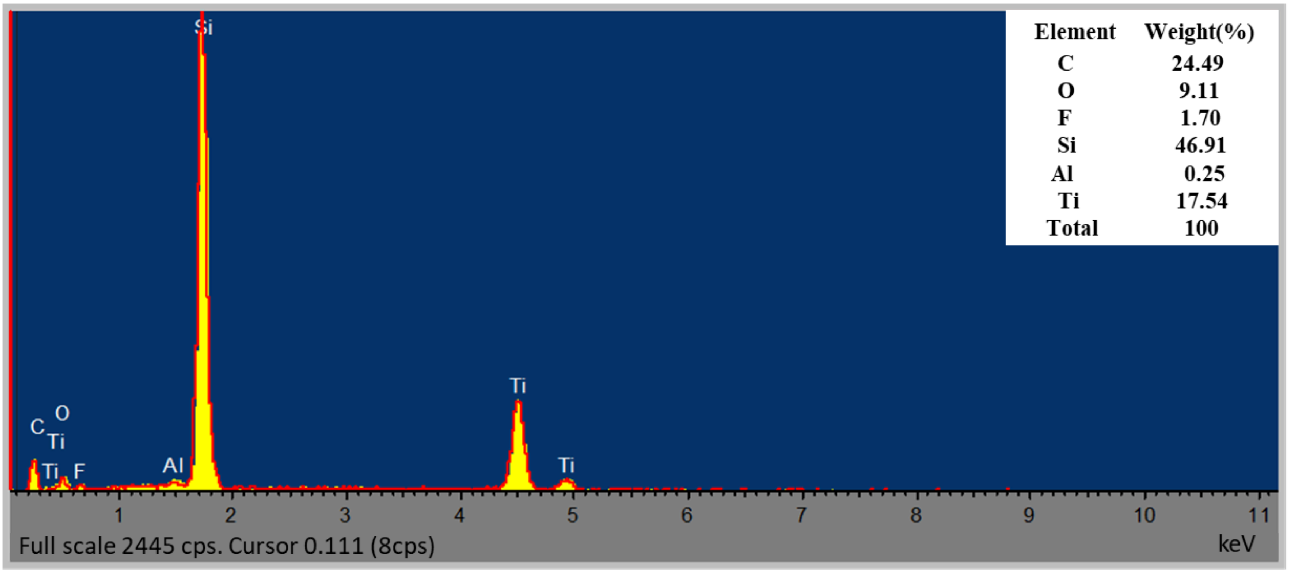


Figure 4. Energy-dispersive X-ray spectrum and elemental composition of the MXene@SiC nanocomposite.

The strong Si signal is consistent with the SiC component, while the Ti signal is attributed to the $Ti_3C_2T_x$ MXene framework. The carbon contribution originates from both the MXene structure and SiC. The presence of F can be associated with surface termination groups formed during the HF etching of Ti_3AlC_2. A small amount of Al (0.25 wt%) was detected, indicating a low residual Al content after the etching process.

The EDS results therefore confirm the coexistence of the characteristic elements of $Ti_3C_2T_x$ MXene and SiC in the synthesized material, supporting the successful formation of the MXene@SiC nanocomposite. These findings confirm the successful fabrication and superior electrochemical performance of the MXene@SiC/GCE. The electrochemical active surface area (ECSA) was calculated using the Randles–Sevcik equation: $Ip = 2.69 \times 10^5$ A $D^{1/2}$ $n^{3/2}$ $\upsilon^{1/2}$ C where A is the electrochemical surface area of the electrode, n is the number of electrons involved in the redox reaction, D is the diffusion coefficient of the molecule in solution (6.67×10^{-6} cm^2 s^{-1} for ferricyanide), C is the concentration of ferricyanide, and υ is the scan rate. The calculated electrochemical surface areas of GCE, MXene@SiC/GCE were 0.0707, 0.2823 cm^2, respectively.

2.3. FTIR Characterization

The Fourier-transform infrared (FTIR) spectra of SiC, $Ti_3C_2T_x$ MXene, and the MXene@SiC nanocomposite were recorded to investigate their characteristic surface functional groups and structural interactions, as shown in Figure 5. The FTIR spectrum of SiC exhibits a broad absorption band at 3422.85 cm^{-1}, which can be attributed to O-H stretching vibrations associated with surface hydroxyl groups or adsorbed moisture. The band at 1643.58 cm^{-1} is related to the bending vibration of molecular water. Additional absorption bands are observed at 1200.35 and 942.07 cm^{-1}, while the band at 584.94 cm^{-1} can be associated with the characteristic vibrations of the Si–C framework.

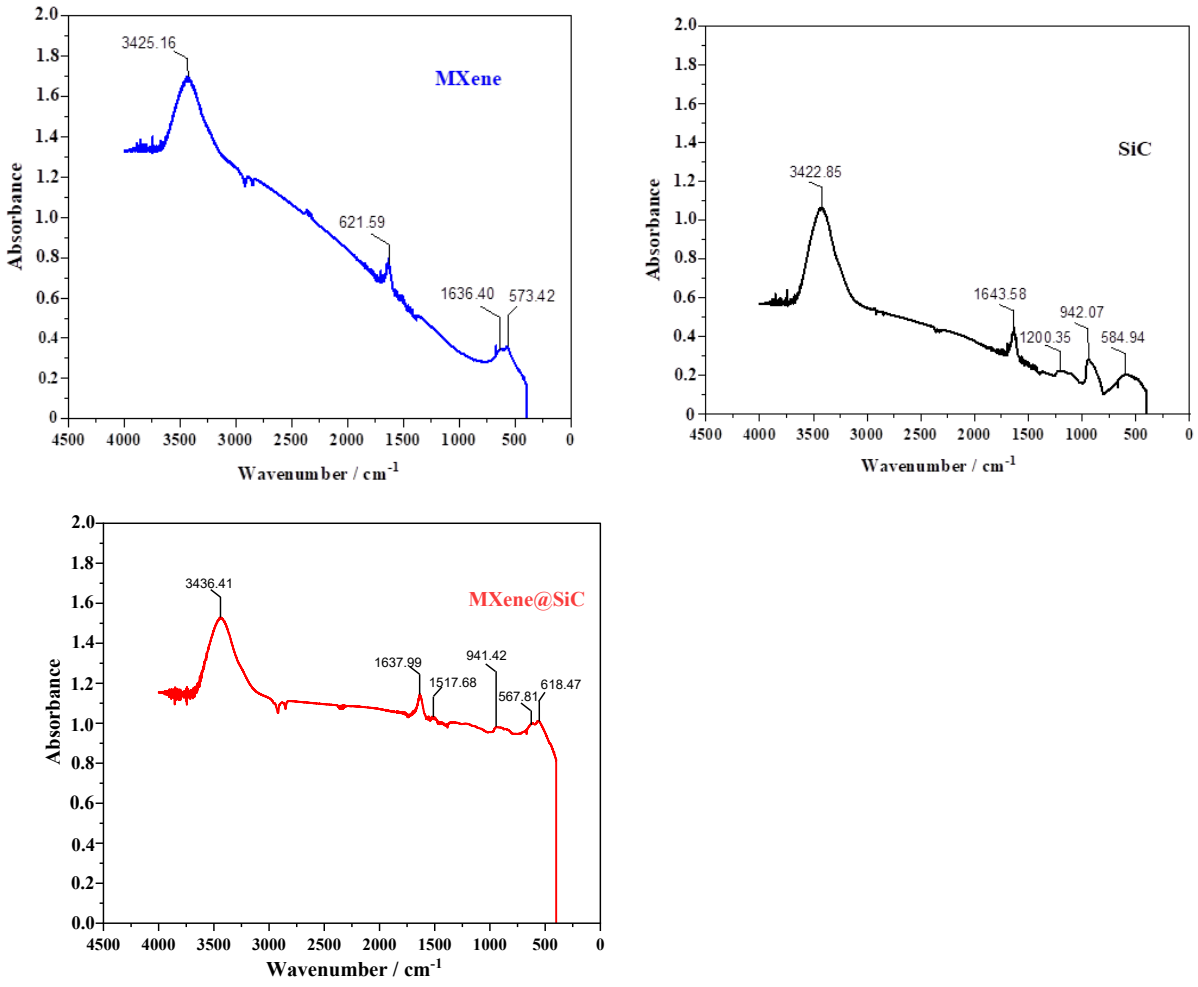


Figure 5. FTIR spectra of SiC, $Ti_3C_2T_x$ MXene, and the MXene@SiC nanocomposite.

The spectrum of $Ti_3C_2T_x$ MXene shows a broad band centered at 3425.16 cm^{-1}, corresponding to O-H stretching vibrations. The absorption feature at 1636.40 cm^{-1} is related to the bending vibration of adsorbed water. The bands observed at 621.59 and 573.42 cm^{-1} are associated with vibrations within the $Ti_3C_2T_x$ structure. These features are consistent with the presence of surface functional groups and the characteristic structure of the prepared MXene.

For the MXene@SiC nanocomposite, the broad O-H band appears at 3436.41 cm^{-1}, while the absorption band at 1637.98 cm^{-1} is observed in the lower-wavenumber region. Additional bands are detected at 1517.68, 941.42, 618.47, and 587.81 cm^{-1}. The appearance of characteristic bands from both MXene and SiC in the composite spectrum indicates the coexistence of the two components. The changes in the position and intensity of several absorption bands after combining MXene with SiC suggest an interaction between the two components, supporting the formation of the MXene@SiC nanocomposite.

2.4. Cyclic Voltammetry and Electrochemical Impedance Spectroscopy

Cyclic voltammetry (CV) and electrochemical impedance spectroscopy (EIS) were employed to investigate the electrochemical characteristics of the bare and modified glassy carbon electrodes. The electrochemical responses of GCE, MXene/GCE, SiC/GCE, and MXene@SiC/GCE were evaluated using a 5 mmol L^{-1} $K_3[Fe(CN)_6]/K_4[Fe(CN)_6]$ redox probe containing 0.1 M KCl. As shown in Figure 6A, all electrodes exhibited distinct anodic and cathodic redox peaks, indicating the occurrence of a reversible electrochemical process. Compared with the bare GCE, the MXene- and SiC-modified electrodes showed enhanced redox responses, confirming the beneficial contribution of the modifying materials to the electrode/electrolyte interface. The anodic peak current increased from (90.00 μA) for the bare GCE to (91.57 μA) for MXene/GCE, (115.125 μA) for SiC/GCE, and (125.85 μA) for MXene@SiC/GCE. Similarly, the absolute cathodic peak current increased from (90.06 μA) to (84.180 μA), (109.932 μA), and (117.069 μA), respectively. The MXene@SiC/GCE exhibited the highest anodic and cathodic peak currents among the investigated electrodes. This enhanced response can be associated with the combined contribution of the highly conductive MXene layers and SiC, which provides a favorable surface for electron transfer and increases the electrochemically accessible area of the electrode. The anodic and cathodic peak potentials were (Epa = 0.272 V, Epc = 0.179 V) for the bare GCE, (Epa = 0.281 V, Epc = 0.170 V) for MXene/GCE, (Epa = 0.285 V, Epc = 0.170 V) for SiC/GCE, and (Epa = 0.293 V, Epc = 0.177 V) for MXene@SiC/GCE. The corresponding peak-to-peak separation values were (ΔEp = 0.093 V), (0.111 V), (0.115 V), and (0.116 V), respectively. Although the peak currents increased after electrode modification, the slight increase in ΔEp indicates that the modification did not improve the electrochemical reversibility of the redox process. Overall, the improved peak current response of MXene@SiC/GCE demonstrates the complementary contribution of the two components in constructing an effective electrode interface.

EIS measurements were further performed to examine the interfacial electrochemical behavior of the prepared electrodes. The corresponding Nyquist plots are presented in Figure 6B. The impedance responses of the modified electrodes differed from that of the bare GCE, indicating changes in the electrode/electrolyte interfacial properties after surface modification. The MXene@SiC-modified electrode displayed a distinct impedance profile compared with the individual MXene- and SiC-modified electrodes, confirming that the formation of the hybrid nanocomposite alters the interfacial charge-transport characteristics. The nearly linear portions observed in the Nyquist plots are associated with diffusion-related processes at the electrode/electrolyte interface. Overall, the CV and EIS results confirm

that modification of the GCE with MXene@SiC substantially changes its electrochemical behavior and provides a favorable interface for subsequent Cd(II) detection.

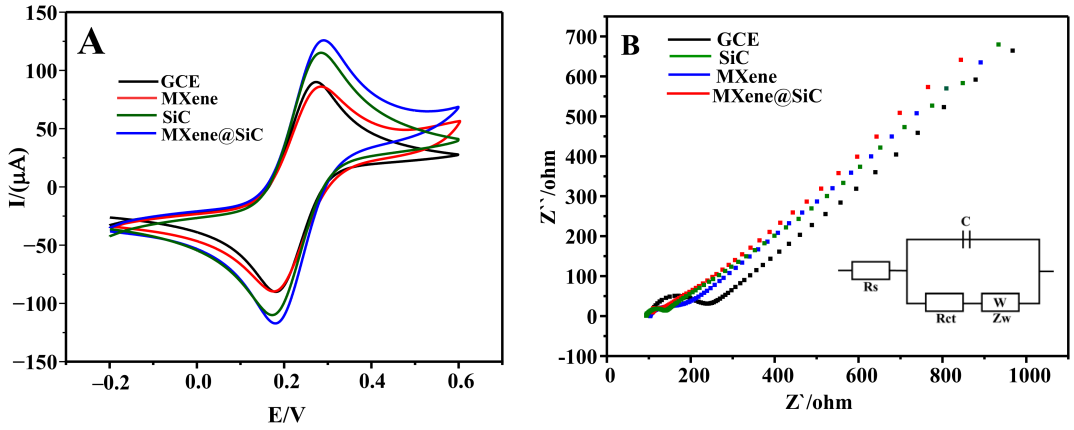


Figure 6. (**A**) Cyclic voltammograms and (**B**) Nyquist plots of bare GCE, MXene/GCE, SiC/GCE, and MXene@SiC/GCE in 5 mmol L^{-1} $K_3[Fe(CN)_6]/K_4[Fe(CN)_6]$ solution containing 0.1 M KCl.

2.5. Electrochemical Response of Cd (II) on the Modified Electrodes

In this experiment, differential pulse voltammetry (DPV) was employed to compare the electrochemical response of Cd(II) at the bare glassy carbon electrode (GCE) and MXene@SiC-modified GCE. A 400 μg/L Cd(II) solution was analyzed under the optimized experimental conditions. As shown in Figure 7, both electrodes exhibited a distinct Cd (II) stripping peak at approximately −0.84 V. However, the MXene@SiC/GCE produced a substantially higher peak current of approximately 58.4 μA, whereas the bare GCE showed a response of about 20.2 μA. The significant enhancement in the current response demonstrates the beneficial effect of modifying the electrode surface with the MXene@SiC nanocomposite. This improvement can be attributed to the high electrical conductivity and large electrochemically accessible surface of MXene, together with the contribution of SiC to the surface structure of the composite. The presence of MXene surface functional groups may also promote the interaction and accumulation of Cd(II) ions at the electrode interface. Therefore, the markedly enhanced stripping response obtained with the MXene@SiC/GCE confirms the effectiveness of the nanocomposite modification for Cd(II) electrochemical detection.

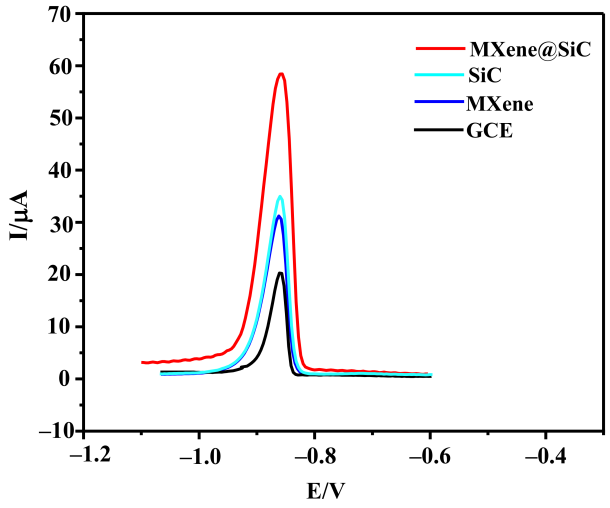


Figure 7. Differential pulse voltammograms of bare GCE and MXene@SiC/GCE for the determination of 400 μg/L Cd(II) under optimized experimental conditions.

2.6. Effect of Cd (II) Concentration

The analytical response of the MXene@SiC-modified electrode was evaluated by varying the Cd(II) concentration from 0.5 to 1000 µg/L. With an increase in Cd(II) concentration, a gradual enhancement of the stripping peak current was observed, while a distinct electrochemical peak appeared at approximately −0.9 V. The progressive increase in the peak current can be attributed to the greater accumulation of Cd(II) ions at the active sites of the modified electrode as their concentration in the solution increases. This concentration-dependent behavior confirms the effective interaction between Cd(II) ions and the MXene@SiC-modified electrode surface. The DPV responses of the MXene@SiC-modified electrode at different Cd(II) concentrations and the corresponding calibration plots are presented in Figure 8. The black square symbols represent the experimental data points, while the red lines indicate the corresponding linear regression fits.

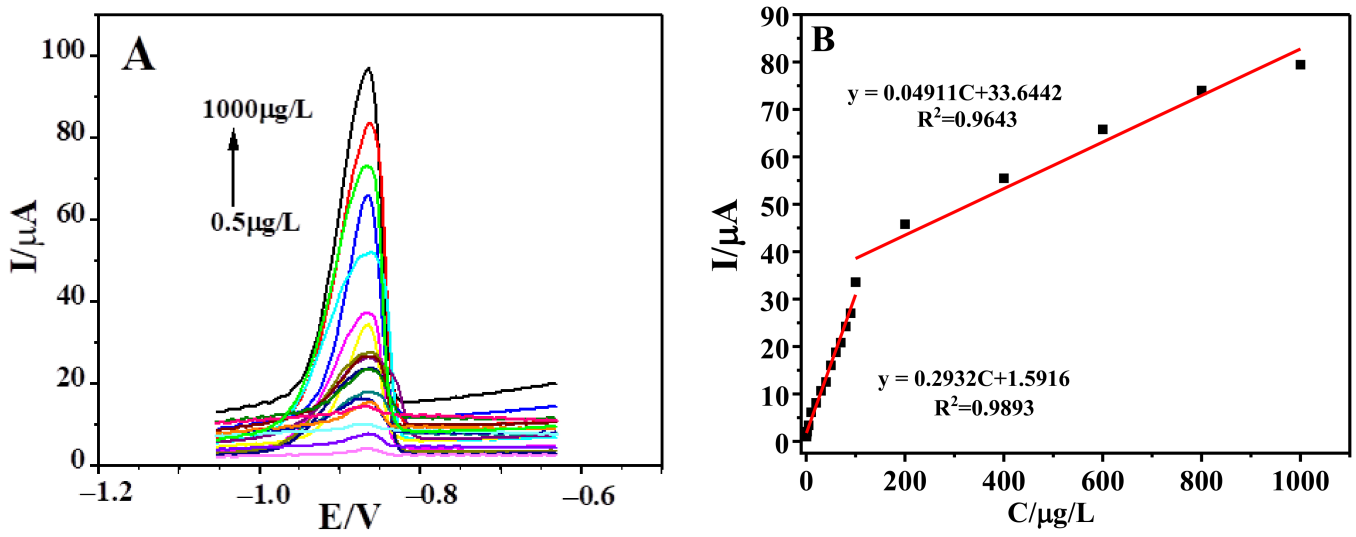


Figure 8. (**A**) Differential pulse voltammograms of Cd(II) at different concentrations from 0.5 to 1000 µg/L using the MXene@SiC-modified electrode; (**B**) corresponding calibration plots of peak current versus Cd(II) concentration.

A quantitative relationship between the Cd(II) concentration and the corresponding peak current was further established. The calibration plot demonstrates two distinct linear concentration ranges. In the lower concentration region, the linear regression equation was $I = 0.2932C + 1.5916$, with a correlation coefficient of $R^2 = 0.9893$. At higher Cd(II) concentrations, the calibration curve followed the equation $I = 0.04911C + 33.6442$, with $R^2 = 0.9643$. The considerably higher slope observed in the lower concentration range indicates a stronger current response toward small changes in Cd(II) concentration.

The difference in the slopes between the two linear regions may be related to the progressive occupation of the electrochemically active sites on the MXene@SiC surface. At relatively low Cd(II) concentrations, a larger proportion of the available active sites remains unoccupied, allowing efficient accumulation of Cd(II) ions and resulting in a higher sensitivity. With further increases in concentration, the active sites become increasingly occupied, leading to a gradual reduction in the rate of current increase. Nevertheless, the observed concentration-dependent response demonstrates that the MXene@SiC-modified electrode is capable of providing a measurable electrochemical signal over a broad Cd(II) concentration range.

2.7. Influence of pH

The influence of the supporting electrolyte pH on the electrochemical response of the MXene@SiC-modified electrode toward Cd(II) was investigated over the pH range of 2–7. Noticeable changes in the differential pulse voltammetric response were observed as the pH of the solution was varied. When the pH was gradually increased from 2 to 5, the Cd(II) stripping peak current increased continuously and reached its highest value at pH 5. However, further elevation of the pH caused a significant reduction in the peak current, with the lowest response observed at pH 7.

In addition to the peak current, the effect of pH on the Cd(II) peak potential E_{pa} was also examined. As shown in Figure 9C, the peak potential shifted toward more negative values with increasing pH. Linear regression of the E_{pa}–pH plot yielded the equation $E_{pa} = -0.0216\,\mathrm{pH} - 0.7725$, with a coefficient of determination of ($R^2 = 0.91$). The slope of −21.6 mV/pH is lower in magnitude than the theoretical Nernstian value of approximately 59 mV/pH at 25 °C. This pH-dependent potential shift may indicate the involvement of protons in the electrochemical process; however, the slope alone does not provide sufficient evidence to establish a definitive proton-coupled electron-transfer mechanism.

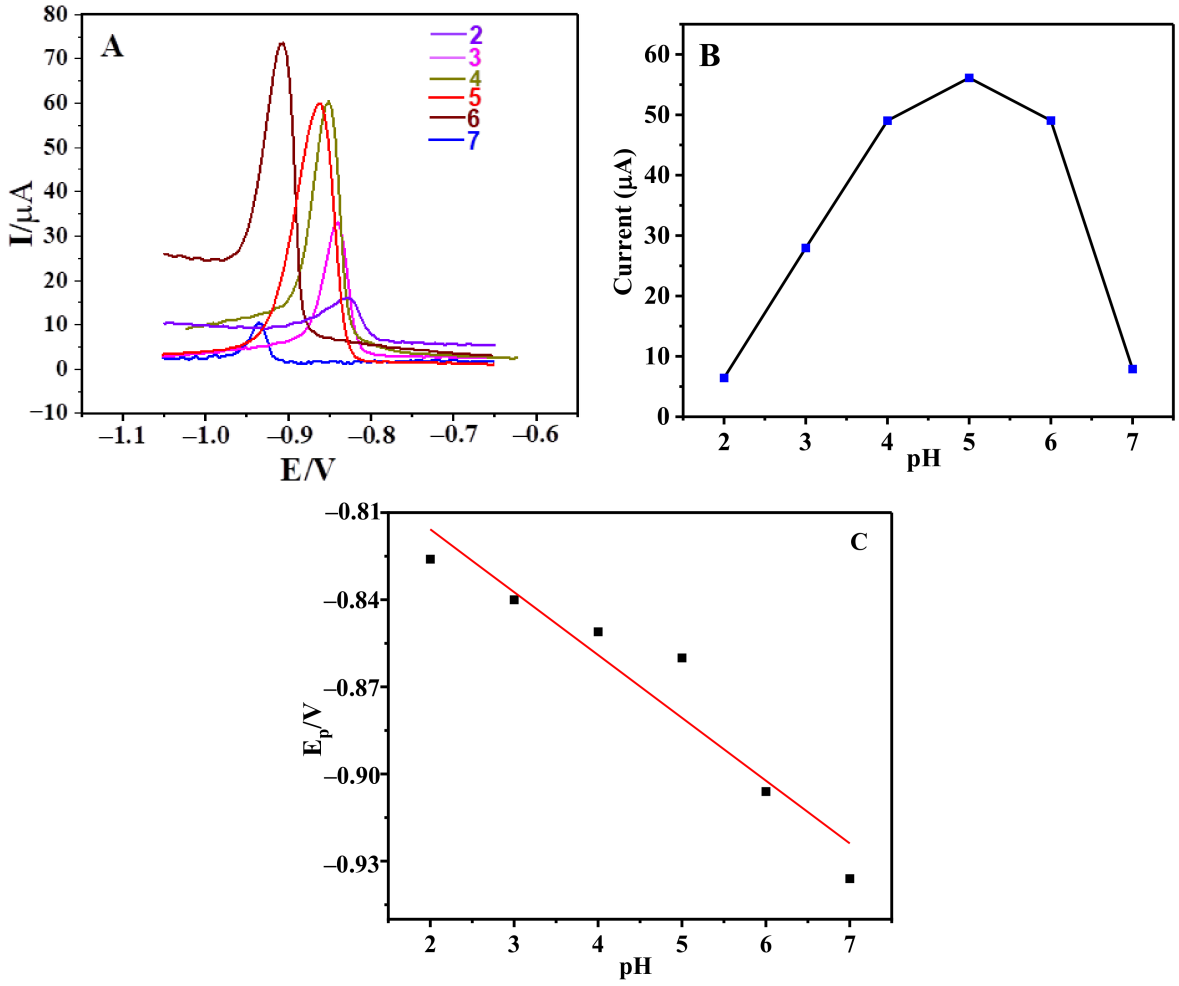


Figure 9. (**A**) Differential pulse voltammograms of Cd(II) at different pH values (2–7) using the MXene@SiC-modified electrode; (**B**) dependence of the Cd(II) peak current on solution pH; (**C**) variation in the Cd(II) peak potential (E_p) with pH.

The corresponding dependence of the peak current on pH demonstrates a clear maximum at pH 5, indicating that this medium provides favorable conditions for the accumula-

tion and subsequent electrochemical stripping of Cd(II) ions on the MXene@SiC-modified electrode. Under strongly acidic conditions, the relatively high concentration of H^+ ions may compete with Cd(II) ions for available surface-active sites, thereby limiting Cd(II) accumulation and decreasing the measured current. As the pH becomes higher, changes in the chemical form and surface interaction of Cd(II) may adversely affect its electrochemical response. Therefore, pH 5 was selected as the optimized condition for the subsequent determination of Cd(II) ions.

2.8. Effect of Accumulation Time

The effect of accumulation time on the Cd(II) stripping response of the MXene@SiC-modified electrode was examined within the range of 50–500 s. The corresponding differential pulse voltammograms demonstrate a gradual enhancement of the Cd(II) peak current with increasing accumulation time, as shown in Figure 10A. At shorter accumulation times, the recorded current is relatively low, which can be attributed to the limited amount of Cd(II) accumulated on the electrode surface. As the accumulation period is extended, more Cd(II) ions are retained at the active sites of the MXene@SiC composite, resulting in a pronounced increase in the stripping peak current.

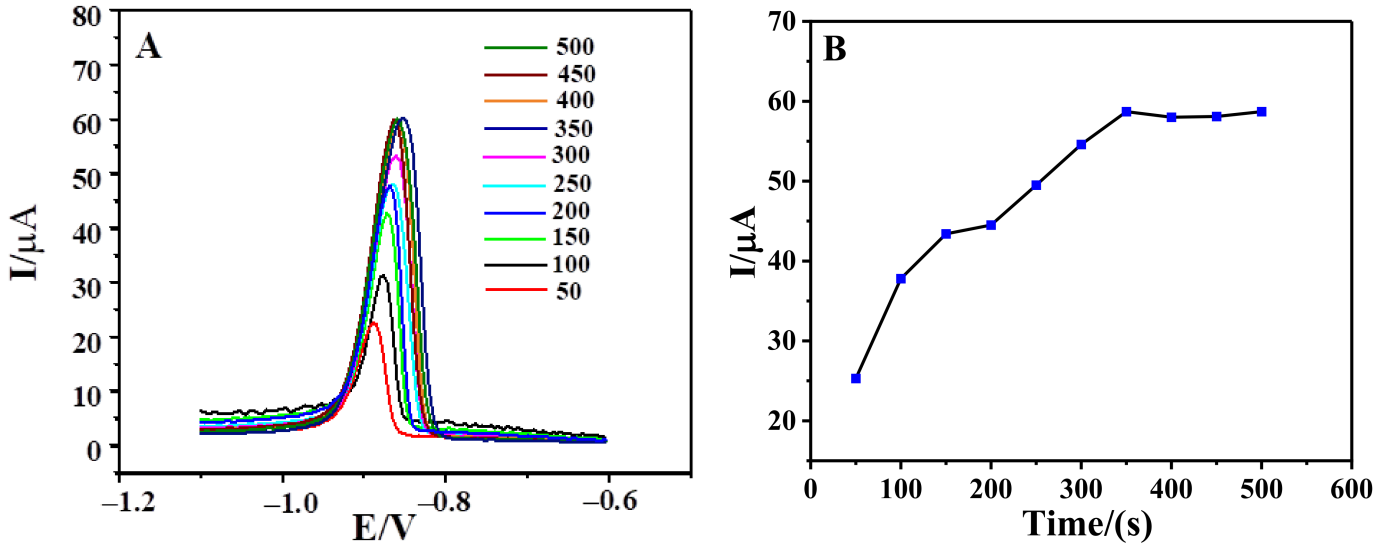


Figure 10. (**A**) Differential pulse voltammograms of Cd(II) at the MXene@SiC-modified electrode at different accumulation times: 50, 100, 150, 200, 250, 300, 350, 400, 450, and 500 s; (**B**) dependence of the peak current on accumulation time.

A rapid increase in the analytical signal is observed between 50 and 350 s, after which the current response changes only slightly. The maximum peak current is reached at approximately 350 s, indicating that sufficient Cd(II) ions have accumulated on the modified electrode surface under this condition. When the accumulation time is further increased to 400 and 500 s, no substantial enhancement of the peak current is observed. This tendency suggests that most of the accessible active sites gradually become occupied by Cd(II) ions and that the electrode surface approaches an adsorption equilibrium.

The relationship between the peak current and accumulation time, presented in Figure 10B, confirms this behavior. Initially, the signal increases markedly with increasing accumulation time, whereas after approximately 350 s, the response becomes nearly constant.

Such a plateau can be associated with the progressive saturation of available binding sites on the MXene@SiC-modified electrode. Once the surface reaches a near-equilibrium

state, extending the accumulation period provides only a limited increase in the amount of Cd(II) accumulated.

Considering both the increase in peak current and the stabilization of the response at longer accumulation periods, an accumulation time of 350 s was selected as the optimum condition for subsequent Cd(II) measurements. This condition provides a sufficiently strong analytical signal while avoiding unnecessary extension of the measurement procedure.

2.9. Effect of Deposition Potential

The Cd(II) stripping response was investigated at different deposition potentials ranging from −1.5 to −1.0 V using the MXene@SiC-modified electrode. The voltammograms show a distinct stripping peak near −0.85 V, while the peak current varies with the applied deposition potential. As the deposition potential shifted from −1.5 to −1.2 V, the peak current increased considerably and reached its maximum at −1.2 V. Further shifting the potential toward −1.0 V resulted in a slight decrease in the current response. The corresponding differential pulse voltammograms and the dependence of the Cd(II) peak current on deposition potential are presented in Figure 11. The blue square symbols in (b) represent the experimental data points.

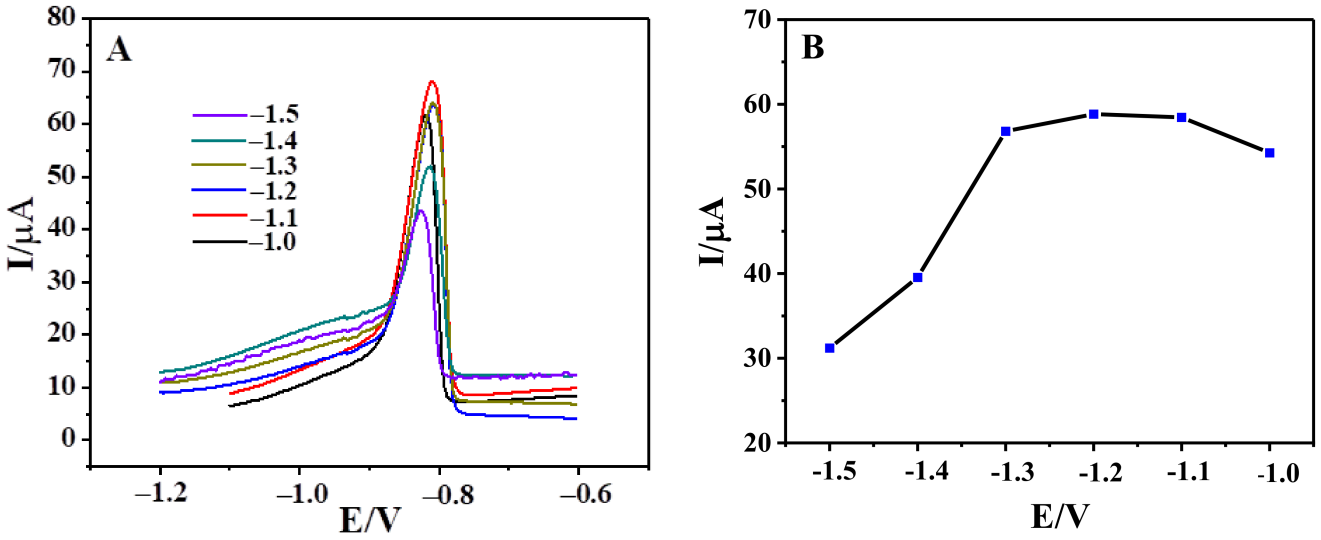


Figure 11. (**A**) Differential pulse voltammograms of Cd(II) obtained at different deposition potentials ranging from −1.5 to −1.0 V using the MXene@SiC-modified electrode; (**B**) dependence of the Cd(II) peak current on the deposition potential.

The dependence of the Cd(II) peak current on the deposition potential shows that the maximum analytical response was obtained at −1.2 V. This behavior indicates that −1.2 V provides suitable conditions for the effective accumulation of Cd(II) on the MXene@SiC-modified electrode surface. Therefore, −1.2 V was selected as the optimum deposition potential for subsequent electrochemical determination of Cd(II) ions.

2.10. Influence of Scan Rate

The electrochemical behavior of the MXene@SiC-modified electrode was investigated by cyclic voltammetry at different scan rates ranging from 10 to 120 mV s^{-1}. A pair of well-defined anodic and cathodic peaks corresponding to the $[Fe(CN)_6]^{3-}/[Fe(CN)_6]^{4-}$ redox couple was observed throughout the investigated scan-rate range. With increasing scan rate, both anodic and cathodic peak currents increased progressively, demonstrating the enhanced electrochemical response of the modified electrode. A slight shift in the peak potentials was also observed at higher scan rates, which may be related to the kinetics of

electron transfer at the electrode–solution interface. The cyclic voltammograms recorded at different scan rates and the corresponding relationships between the anodic and cathodic peak currents and the square root of the scan rate are presented in Figure 12.

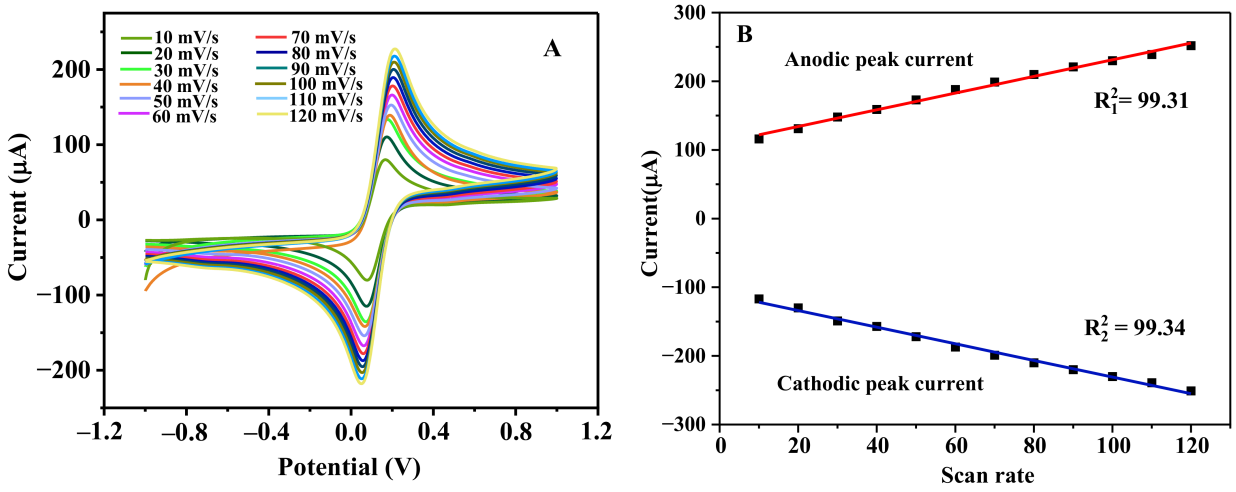


Figure 12. (**A**) Cyclic voltammograms of the MXene@SiC-modified electrode recorded at scan rates from 10 to 120 mV s^{-1}; (**B**) plots of anodic and cathodic peak currents versus the square root of the scan rate (v) in 5 mmol L^{-1} $K_3[Fe(CN)_6]/K_4[Fe(CN)_6]$ solution containing 0.1 M KCl. The black square symbols represent the experimental data points, while the red and blue lines indicate the corresponding linear regression fits for the anodic and cathodic peak currents, respectively.

The dependence of the peak currents on the square root of the scan rate ($\nu^{1/2}$) was further examined. Both the anodic and cathodic peak currents exhibited an approximately linear relationship with $\nu^{1/2}$, with correlation coefficients of $R^2 = 0.9931$ and $R^2 = 0.9934$, respectively. The good linear correlation suggests that the electrochemical process occurring at the MXene@SiC-modified electrode is mainly governed by diffusion of the electroactive species toward the electrode surface.

The progressive increase in peak current with scan rate can be associated with a higher flux of the redox-active species to the electrode interface during faster potential scanning. The well-defined voltammetric profiles and high linearity observed for both oxidation and reduction currents indicate stable electrochemical behavior of the modified electrode within the investigated scan-rate range. These findings further demonstrate that the MXene@SiC nanocomposite provides an electrochemically active interface suitable for efficient electron-transfer processes.

2.11. Selectivity and Stability of the MXene@SiC/GCE

The selectivity of the developed sensor was evaluated to investigate the influence of potentially interfering substances on the electrochemical response toward Cd(II). A 400 μg/L Cd(II) solution was used as the reference, and the effects of $NaNO_2$, $CaCl_2$, $MnSO_4$, $ZnSO_4$, $CuSO_4$, and $PbSO_4$ were examined under the optimized experimental conditions. As shown in Figure 13, the response obtained for Cd(II) was taken as 100%, while the relative responses in the presence of $NaNO_2$, $CaCl_2$, $MnSO_4$, Zn(II), Cu(II), and Pb(II) were 98.71%, 98.91%, 96.97%, 96.5%, 95.2%, and 95.7%, respectively. The small variation in the current response indicates that the investigated interfering species caused only a minor change in the Cd(II) signal. The limited influence of Zn(II), Cu(II), and Pb(II) may be partly attributed to the separation of their stripping peak potentials from that of Cd(II), which minimizes peak overlap under the applied experimental conditions. These results

indicate that the MXene@SiC-modified electrode exhibits favorable selectivity toward Cd(II) in the presence of the tested interfering species.

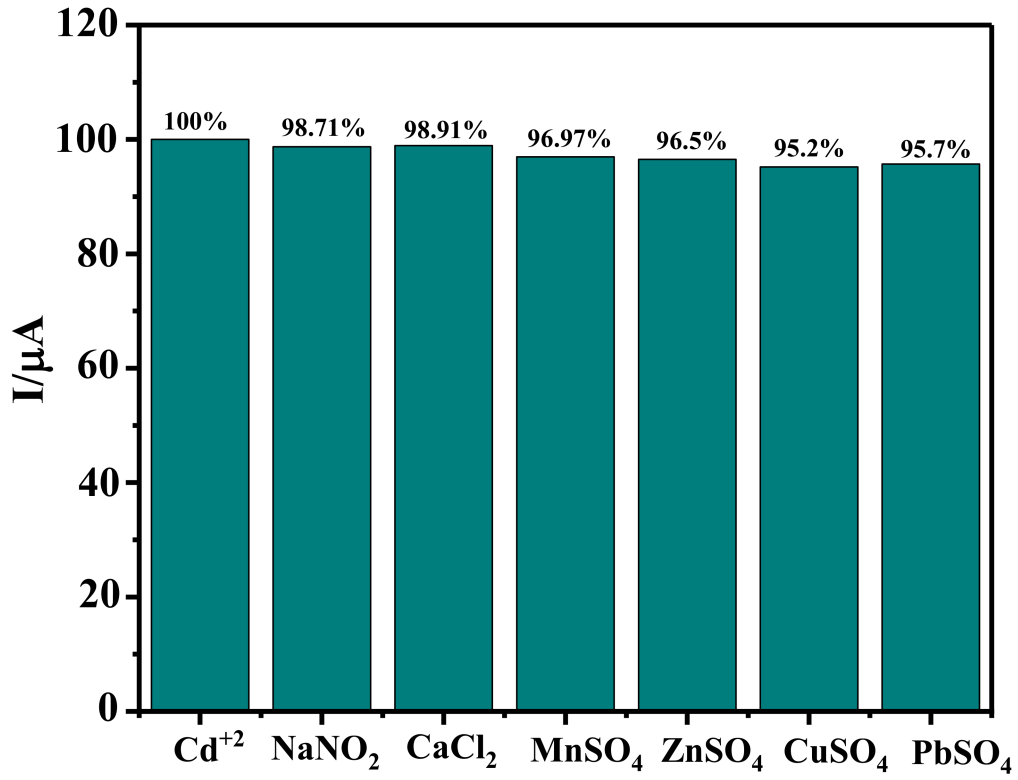


Figure 13. Effect of different interfering substances on the electrochemical response of the MXene@SiC/GCE toward 400 μg/L Cd(II).

The storage stability of the proposed MXene@SiC-modified electrode was evaluated using three electrodes stored at 4 °C. The electrodes were tested for Cd(II) detection after 3, 5, and 7 days of storage. The results demonstrated that the electrochemical signal of the MXene@SiC/GCE retained more than 98% of its initial value after 7 days of storage. This result indicates good short-term storage stability of the proposed sensor under refrigerated conditions.

2.12. Real Sample Detection

To evaluate the practical applicability of the developed sensor, the concentration of Cd(II) in a tap water sample was determined using the standard addition method. The tap water sample was analyzed under the optimized experimental conditions, including pH 5.0, an accumulation time of 350 s, and a deposition potential of −1.2 V. Known amounts of Cd(II) at concentrations of 5, 50, 300, and 700 μg/L were added to the water sample, and the corresponding electrochemical responses were recorded. All measurements were performed in triplicate ($n = 3$). To further evaluate the analytical performance of the proposed MXene@SiC-modified electrode, its performance was compared with those of previously reported electrochemical sensors for Cd(II) detection. As summarized in Table 1, the MXene@SiC/GCE exhibits a broader working concentration range (0.5–1000 μg/L) and a lower reported limit of detection (LOD) of 0.25 μg/L than the selected comparison electrodes. These results indicate the potential of the MXene@SiC composite for Cd(II) determination over a wide concentration range. The combination of MXene and SiC may contribute to the observed analytical performance of the modified electrode.

Table 1. Comparison of the analytical performance of the proposed sensor with previously reported electrochemical sensors for Cd(II) detection.

Sensing Electrodes	Platform	Technique	Linear Range (μg/L)	LOD (μg/L)	Sensitivity	Sample Matrix	References
Nafion-Bismuth/SPGE	Gold SPGE	Anodic stripping square-wave voltammetry	50–300	4	Not reported	River and tap water	[5]
Bi oxycarbide/GCE	GCE	DPASV	10–50	4.24	Not reported	Water samples	[38]
MWCNT/BiOCl/GCE	GCE	SWASV	10–50	1.19	Not reported	Sediment pore water	[8]
ALA/PDA/rGO/GCE	GCE	DPV	3–10	2.86	0.0929 μA/(μg/L)	Real water samples	[9]
MXene@SiC/GCE (this work)	GCE	DPV	0.5–1000	0.25	0.2932 and 0.04911 μA/(μg/L)	Tap water	This work

As presented in Table 2, the recovery values ranged from 98.22% to 114.6%, while the relative standard deviation (RSD) values ranged from 0.160% to 1.34%. The highest recovery (114.6%) was observed at the lowest Cd(II) addition level (5 μg/L), indicating a possible positive bias. This deviation may be associated with matrix effects or increased relative measurement uncertainty at low analyte concentrations. At higher addition levels, the recovery values were 98.6%, 98.22%, and 100.1% for 50, 300, and 700 μg/L, respectively. The low RSD values indicate good repeatability of the measurements. Overall, these results demonstrate the potential applicability of the MXene@SiC-modified electrode for Cd(II) determination in tap water samples.

Table 2. Determination of Cd(II) in a real water sample using the MXene@SiC-modified electrode. (n = 3).

№	Added	I/μA	Found	Recovery %	RSD %
1	5 μg/L	3.31	5.73 ± 0.07	114.6	1.34
2	50 μg/L	15.97	49.03 ± 0.54	98.6	1.117
3	300 μg/L	47.45	294.68 ± 1.84	98.22	0.627
4	700 μg/L	68.04	700.5 ± 1.12	100.1	0.160

3. Materials and Methods

3.1. Chemicals and Reagents

Hydrofluoric acid (HF, 40 wt%), nitrogen gas (N_2), potassium ferrocyanide ($K_4[Fe(CN)_6]$), potassium ferricyanide ($K_3[Fe(CN)_6]$), dimethyl sulfoxide (DMSO), and potassium chloride (KCl) were purchased from Sinopharm Chemical Reagent Co., Ltd. (Shanghai, China). All reagents were of analytical grade and used as received without further purification.

The electrochemical experiments were conducted in a solution of 5 mmol/L $K_3[Fe(CN)_6]/K_4[Fe(CN)_6]$ and 0.1 M KCl. This redox pair solution is well suited for studying the electrochemical redox behavior of the synthesized material. The pH of the solution was adjusted to the desired value using hydrochloric acid and sodium hydroxide solutions. The buffer solution was prepared by mixing 0.2 mol/L CH_3COONa and CH_3COOH. The CH_3COONa/CH_3COOH buffer solution was stored at room temperature, with pH adjustments made by adding appropriate amounts of acetic acid solution, sodium acetate, or sodium hydroxide solution.

3.2. Apparatus

Electrochemical measurements, such as cyclic voltammetry (CV) and electrochemical impedance spectra (EIS), were performed using a CS Patentiostat/Galvanostat (Wuhan CorrTest Instruments Co., Ltd., Wuhan, China). A standard three-electrode cell was used, with a glassy carbon electrode (GCE) (surface area 3 mm) as the working electrode, an Ag/AgCl electrode (saturated with KCl) as the reference electrode, and a platinum wire as the counter electrode. All potentials mentioned in the experimental results were referenced to the standard Ag/AgCl (KCl-saturated) reference electrode. The surface morphology of the synthesized materials was characterized by scanning electron microscopy (SEM). SEM micrographs were obtained using a SEM3200 Det ETD-SE scanning electron microscope (CIQTEK Co., Ltd., Hefei, China) at an accelerating voltage of 10 kV. In addition, SEM images of the fabricated films were obtained using a ZEISS Ultra 55 scanning electron microscope (Carl Zeiss AG, Oberkochen, Germany).

3.3. Preparation of the $Ti_3C_2T_x$ MXene and MXene@SiC Nanocomposite

$Ti_3C_2T_x$ MXene was prepared by selective etching of Al from Ti_3AlC_2 using 40% HF. The Ti_3AlC_2 powder was treated with HF under continuous stirring for 24 h. After etching, the suspension was centrifuged at 4000 rpm for 5 min, and the supernatant was removed. The washing and centrifugation procedures were repeated using deionized water until the pH of the supernatant reached approximately 6. The obtained material was subsequently treated with DMSO under continuous stirring to promote interlayer separation and facilitate the formation of $Ti_3C_2T_x$ MXene. The resulting MXene was collected and used for the preparation of the nanocomposite (Figure 14).



Figure 14. Schematic illustration of the preparation of $Ti_3C_2T_x$ MXene by HF etching of Ti_3AlC_2.

The MXene@SiC nanocomposite was prepared by mixing $Ti_3C_2T_x$ MXene and SiC at a 1:1 mass ratio. The two components were combined and dispersed in DMSO under continuous stirring to obtain a homogeneous suspension. This mixing process promotes intimate contact between the layered MXene structure and SiC particles. The resulting suspension was collected and dried to obtain the MXene@SiC nanocomposite, which was subsequently used for structural characterization and modification of the glassy carbon electrode (Figure 15).

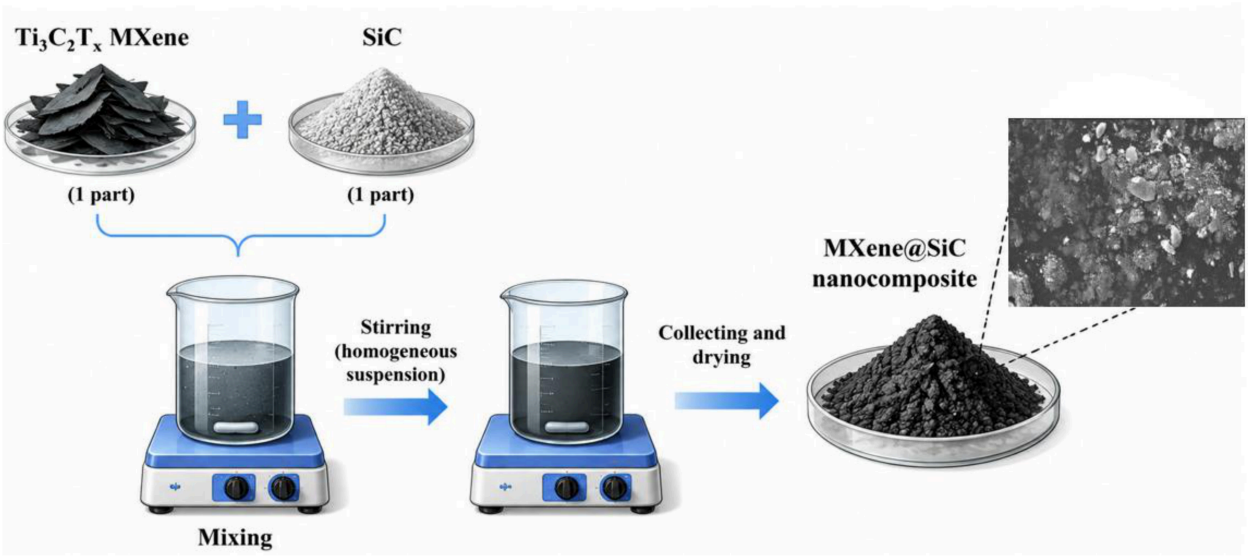


Figure 15. Schematic illustration of the preparation of the MXene@SiC nanocomposite by mixing $Ti_3C_2T_x$ MXene and SiC at a 1:1 mass ratio.

3.4. Preparation of the Modified Electrode

The glassy carbon electrode (GCE) was carefully polished using aluminum oxide powders with particle sizes of 1.0, 0.3, and 0.05 μm. The polished electrode was subsequently sonicated for 3 min in a mixture of anhydrous ethanol and distilled water and then dried under a nitrogen stream.

For electrode modification, 9 mg of the MXene@SiC nanocomposite was dispersed in 1 mL of ethanol and 2 mL of distilled water. The obtained suspension was continuously stirred for 30 min to achieve a uniform dispersion of the nanocomposite. Subsequently, 5 μL of the prepared suspension was drop-cast onto the surface of the pre-cleaned GCE. The electrode was allowed to dry at room temperature for 15 min, yielding the MXene@SiC/GCE for subsequent electrochemical measurements.

3.5. The Electrochemical Detection Procedure

A CS Potentiostat/Galvanostat (Electrochemical Workstation) with a three-electrode system was used for the experiments. The working electrode (WE) was a Glassy Carbon Electrode (GCE), the reference electrode (RE) was an Ag/AgCl electrode, and the counter electrode (CE) was a platinum electrode. The chemical behavior of heavy metals on the electrode was characterized by cyclic voltammetry (CV) and differential pulse voltammetry (DPV).

Compared to CV, DPV offers higher sensitivity, lower detection limits, and effectively suppresses background currents. Table 3 lists of the instruments required for the experiment.

Table 3. Experimental parameters used for electrochemical measurements.

Detection Method	Potential Range	Frequency Range	Scanning Speed	Sampling Interval	Frequency
Cyclic voltammetry	−0.2–+ 0.6 V	-	50 mV/s	0.001 V	-
Differential pulse voltammetry	−1.2–−0.6 V	-	-	0.1 V	20 HZ
Electrochemical interference spectroscopy (EIS)	-	0.1 Hz–100 Hz	-	-	-

The electrochemical interference spectroscopy method is carried out in a 0.1 mol/L potassium ferricyanide/potassium ferricyanide ($K_3[Fe(CN)_6]/K_4[Fe\ (CN)_6]$) (1:1) solution with a frequency range from 0.1 Hz to 100 Hz. Table 3 summarizes the electrochemical measurement conditions. Formula 1 calculates the detection limit of lead ions (Cm).

There, m—slope of the linear calibration curve, Sb—relative standard deviation of the results of 20 parallel experiments in acetic acid and sodium acetate buffer.

4. Conclusions

In this study, a MXene@SiC nanocomposite-modified glassy carbon electrode (MXene@SiC/GCE) was successfully fabricated and investigated for the electrochemical determination of Cd(II) ions in aqueous samples. The $Ti_3C_2T_x$ MXene and SiC components were combined at a 1:1 mass ratio to construct a hybrid nanocomposite with favorable electrochemical characteristics. The successful formation and composition of the prepared material were supported by SEM, EDS, and FTIR characterization. The morphological and spectroscopic results confirmed the presence of the characteristic components of MXene and SiC within the composite structure. Electrochemical characterization using cyclic voltammetry demonstrated that the MXene@SiC/GCE exhibited a stronger redox response than the bare GCE, MXene/GCE, and SiC/GCE. The enhanced response indicates that incorporation of MXene and SiC substantially modifies the electrochemical properties of the electrode surface. The combined contribution of the conductive $Ti_3C_2T_x$ MXene layers and SiC provides a favorable interface for electron transfer and electrochemical reactions. Electrochemical impedance spectroscopy further confirmed changes in the interfacial charge-transfer behavior after modification of the GCE surface with the MXene@SiC nanocomposite.

The influence of the scan rate was also investigated, and the peak current increased with increasing scan rate. The corresponding linear relationships between peak current and the square root of the scan rate, with R^2 values of 0.9931 and 0.9934, indicated that the electrochemical process was predominantly diffusion-controlled. Optimization of the experimental parameters showed that pH 5, an accumulation time of 350 s, and a deposition potential of −1.2 V provided favorable conditions for Cd(II) determination. Under these conditions, the MXene@SiC/GCE exhibited a well-defined Cd(II) stripping peak at approximately −0.84 V.

The comparison between the bare and modified electrodes further demonstrated the effectiveness of the MXene@SiC modification. For a 400 μg/L Cd(II) solution, the stripping current increased from approximately 20.2 μA at the bare GCE to 58.4 μA at the MXene@SiC/GCE. This pronounced increase in current response can be related to the favorable conductivity and electrochemically accessible surface provided by the hybrid nanocomposite. The surface functional groups associated with $Ti_3C_2T_x$ MXene may additionally contribute to the interaction and accumulation of Cd(II) ions at the electrode interface. The analytical response of the modified electrode showed a concentration-dependent increase in the Cd(II) stripping current over the investigated concentration range. Two linear calibration regions were obtained. In the lower concentration region, the calibration equation was $I = 0.2932C + 1.5916$, with $R^2 = 0.9893$, while the higher concentration region was described by $I = 0.04911C + 33.6442$, with $R^2 = 0.9643$. The difference in slopes between the two regions may be associated with the gradual occupation of available electroactive sites as the Cd(II) concentration increases. The selectivity study also demonstrated that the presence of the investigated interfering substances had only a limited effect on the Cd(II) response. Taking the Cd(II) response as 100%, the relative responses obtained in the presence of $NaNO_2$, $CaCl_2$, and $MnSO_4$ were 98.71%, 98.91%, and 96.97%, respectively. These small variations indicate that the MXene@SiC/GCE maintained a relatively stable response toward Cd(II) in the presence of the tested interfering species. The practical applicability of the developed

electrode was further evaluated using real water samples by the standard addition method. For Cd(II) concentrations of 5, 50, 300, and 700 μg/L, recovery values of 114.6%, 98.6%, 98.22%, and 100.1%, respectively, were obtained, while the corresponding RSD values were 1.34%, 1.117%, 0.627%, and 0.160%. These results indicate satisfactory repeatability and demonstrate that the developed MXene@SiC/GCE can be applied to Cd(II) determination in real aqueous samples.

Overall, the obtained results demonstrate that the MXene@SiC nanocomposite combines the advantageous electrochemical characteristics of $Ti_3C_2T_x$ MXene and SiC and provides an effective modification of the glassy carbon electrode surface. The enhanced current response, favorable selectivity, reproducible analytical performance, and applicability to real water samples demonstrate the potential of this carbon-based hybrid material for electrochemical Cd(II) sensing. The developed MXene@SiC/GCE therefore provides a promising platform for the electrochemical monitoring of cadmium ions in aqueous environmental samples.

Author Contributions: Conceptualization: D.K. and Z.M.; formal analysis: D.K. and N.S. (Nurgul Shadin); investigation: D.K. and Y.T.; methodology: D.K. and Z.M.; supervision: Z.M. and N.S. (Nurgul Shadin); SEM analysis: Y.T.; writing—original draft: D.K.; writing—review and editing: Z.M., N.S. (Nurgul Shadin), Y.B., N.S. (Nazira Sagatbekova), L.W. and Q.Z. All authors have read and agreed to the published version of the manuscript.

Funding: This research was funded by the Abai Kazakh National Pedagogical University (Contract № 05-04/568 dated 21 May 2026 "Advances in MXene Synthesis, Carbon Hybridization, and Their Electrochemical Applications").

Institutional Review Board Statement: Not applicable.

Data Availability Statement: The data presented in this study may be obtained on request from the corresponding author.

Acknowledgments: During the preparation of this manuscript, the authors used ChatGPT (OpenAI, GPT-5.6) for language editing and grammatical correction. In addition, ChatGPT Image Generation (OpenAI) was used to assist in creating and arranging selected schematic and illustrative elements in Figure 1, Figure 2, Figure 14, and Figure 15. The authors reviewed and edited the AI-assisted text and figures and take full responsibility for the accuracy, integrity, and content of this publication. The SEM micrographs incorporated into these figures were obtained experimentally by the authors.

Conflicts of Interest: The authors declare no conflicts of interest.

References

1. Kan, X.; Dong, Y.; Feng, L.; Zhou, M.; Hou, H. Contamination and health risk assessment of heavy metals in China's lead–zinc mine tailings: A meta–analysis. *Chemosphere* **2021**, *267*, 128909. [CrossRef]
2. Perelonia, K.B.S.; Benitez, K.C.D.; Banicod, R.J.S.; Tadifa, G.C.; Cambia, F.D.; Montojo, U.M. Validation of an analytical method for the determination of cadmium, lead and mercury in fish and fishery resources by graphite furnace and Cold Vapor Atomic Absorption Spectrometry. *Food Control* **2021**, *130*, 108363. [CrossRef]
3. Li, B.; Xie, X.; Meng, T.; Guo, X.; Li, Q.; Yang, Y.; Jin, H.; Jin, C.; Meng, X.; Pang, H. Recent advance of nanomaterials modified electrochemical sensors in the detection of heavy metal ions in food and water. *Food Chem.* **2024**, *440*, 138213. [CrossRef]
4. Pizarro, J.; Segura, R.; Tapia, D.; Navarro, F.; Fuenzalida, F.; Aguirre, M.J. Inexpensive and green electrochemical sensor for the determination of Cd(II) and Pb(II) by square wave anodic stripping voltammetry in bivalve mollusks. *Food Chem.* **2020**, *321*, 126682. [CrossRef]
5. Albalawi, I.; Hogan, A.; Alatawi, H.; Moore, E. A sensitive electrochemical analysis for cadmium and lead based on Nafion-Bismuth film in a water sample. *Sens. Bio-Sens. Res.* **2021**, *34*, 100454. [CrossRef]
6. Karazan, Z.M.; Roushani, M. Selective determination of cadmium and lead ions in different food samples by poly (riboflavin)/carbon black-modified glassy carbon electrode. *Food Chem.* **2023**, *423*, 136283. [CrossRef]

7. Albalawi, I.; Hogan, A.; Alatawi, H.; Alsefri, S.; Moore, E. A novel comparative study for simultaneous determination of Cd (II) and Pb (II) based on ruthenium complex-nanoparticles-nafion modified screen-printed gold electrode. *Sens. Actuators B Chem.* **2023**, *380*, 133273. [CrossRef]
8. Cerovac, S.; Guzsvany, V.; Konya, Z.; Ashrafi, A.M.; Svancara, I.; Roncevic, S.; Kukovecz, A.; Dalmacija, B.; Vytras, K. Trace level voltammetric determination of lead and cadmium in sediment pore water by a bismuth-oxychloride particle-multiwalled carbon nanotube composite modified glassy carbon electrode. *Talanta* **2015**, *134*, 640–649. [CrossRef]
9. Patel, M.; Bisht, N.; Prabhakar, P.; Sen, R.K.; Kumar, P.; Dwivedi, N.; Ashiq, M.; Mondal, D.; Srivastava, A.K.; Dhand, C. Ternary nanocomposite-based smart sensor: Reduced graphene oxide/polydopamine/alanine nanocomposite for simultaneous electrochemical detection of Cd^{2+}, Pb^{2+}, Fe^{2+}, and Cu^{2+} ions. *Environ. Res.* **2023**, *221*, 115317. [CrossRef]
10. Mao, D.; Hu, J.; Duan, P.; Qin, C.; Piao, Y. Ultrasensitive and highly reusable electrochemical sensor with ion imprinted nanobiochar. *Sens. Actuators B Chem.* **2022**, *371*, 132490. [CrossRef]
11. Wang, Y.; Wang, L.; Huang, W.; Zhang, T.; Hu, X.; Perman, J.A.; Ma, S. A metal–organic framework and conducting polymer based electrochemical sensor for highperformance cadmium ion detection. *J. Mater. Chem. A* **2017**, *5*, 8385–8393. [CrossRef]
12. Hosseinzadeh, B.; Rodriguez-Mendez, M.L. Electrochemical sensor for food monitoring using metal–organic framework materials. *Chemosensors* **2023**, *11*, 357. [CrossRef]
13. Mukatayeva, Z.S.; Bakytkarim, Y.; Nuerbaheti, W.; Tileuberdi, Y.; Shadin, N.A.; Assirbayeva, Z.M.; Zhussupova, L.A. Electrochemical Sensor based on Silicon Carbide and Coke-Derived Carbon Nanocomposites for Sensitive Detection of Lead Ions. *ES Mater. Manuf.* **2025**, *29*, 1653. [CrossRef]
14. Avchukir, K.; Bakytkarim, Y.; Mukatayeva, Z.S.; Tileuberdi, Y.; Shadin, N.A.; Yenbekova, D.; Rakhymbay, G. High-Sensitivity Detection of Dichlorvos Using a Multi-Walled Carbon Nanotubes-Gold Nanoparticles/Glassy Carbon Electrode Impedimetric Electrochemical Sensor. *Eng. Sci.* **2025**, *38*, 1881. [CrossRef]
15. Mukatayeva, Z.S.; Konarbay, D.; Bakytkarim, Y.; Shadin, N.A.; Tileuberdi, Y. Analytical Determination of Heavy Metals in Water Using Carbon-Based Materials. *Molecules* **2026**, *31*, 5. [CrossRef]
16. Assirbayeva, Z.; Mukatayeva, Z.S.; Shadin, N.A.; Tileuberdi, Y.; Zeng, Q.; Nurakhmetova, A.; Dyussebayev, K.; Sarsekova, K.; Bakytkarim, Y. Synthesis of Carbon Nanomaterial from Coke and Preparation of Copper Oxide-Based Composite. *Molecules* **2026**, *31*, 2129. [CrossRef]
17. Fan, G.; Zhan, J.; Luo, J.; Lin, J.; Qu, F.; Du, B.; Yan, Z. Fabrication of heterostructured Ag/AgCl@g-C_3N_4@UiO-66(NH_2) nanocomposite for efficient photocatalytic inactivation of Microcystis aeruginosa under visible light. *J. Hazard. Mater.* **2021**, *404*, 124062. [CrossRef]
18. Dai, H.; Wang, N.; Wang, D.; Ma, H.; Lin, M. An electrochemical sensor based on phytic acid functionalized polypyrrole/graphene oxide nanocomposites for simultaneous determination of Cd(II) and Pb(II). *Chem. Eng. J.* **2016**, *299*, 150–155. [CrossRef]
19. Qin, X.; Zhang, Z.; Yang, T.; Yuan, L.; Guo, Y.; Yang, X. Auto-fluorescence of cellulose paper with spatial solid phase dispersion-induced fluorescence enhancement behavior for three heavy metal ions detection. *Food Chem.* **2022**, *389*, 133093. [CrossRef]
20. Kalambate, P.K.; Gadhari, N.S.; Li, X.; Rao, Z.; Navale, S.T.; Shen, Y.; Patil, V.R.; Huang, Y. Recent advances in MXene–based electrochemical sensors and biosensors. *TrAC Trends Anal. Chem.* **2019**, *120*, 115643. [CrossRef]
21. Shoaib, M.; Li, H.H.; Khan, I.M.; Zareef, M.; Hassan, M.M.; Niazi, S.; Chen, Q.S. Emerging MXenes-based aptasensors: A paradigm shift in food safety detection. *Trends Food Sci. Technol.* **2024**, *151*, 104635. [CrossRef]
22. Zhang, H.; Wang, Z.; Zhang, Q.; Wang, F.; Liu, Y. Ti_3C_2 MXenes nanosheets catalyzed highly efficient electrogenerated chemiluminescence biosensor for the detection of exosomes. *Biosens. Bioelectron.* **2019**, *124–125*, 184–190. [CrossRef]
23. Zhu, X.; Liu, B.; Hou, H.; Huang, Z.; Zeinu, K.M.; Huang, L.; Yuan, X.; Guo, D.; Hu, J.; Yang, J. Alkaline intercalation of Ti_3C_2 MXene for simultaneous electrochemical detection of Cd(II), Pb(II), Cu(II) and Hg(II). *Electrochim. Acta* **2017**, *248*, 46–57. [CrossRef]
24. Wen, L.; Dong, J.; Yang, H.; Zhao, J.; Hu, Z.; Han, H.; Huo, D. A novel electrochemical sensor for simultaneous detection of Cd^{2+} and Pb^{2+} by MXene aerogel-CuO/carbon cloth flexible electrode based on oxygen vacancy and bismuth film. *Sci. Total Environ.* **2022**, *851*, 158325. [CrossRef]
25. Chen, Y.; Zhao, P.; Hu, Z.; Liang, Y.; Han, H.; Yang, M.; Luo, X.; Hou, C.; Huo, D. Amino-functionalized multilayer $Ti_3C_2T_x$ enabled electrochemical sensor for simultaneous determination of Cd^{2+} and Pb^{2+} in food samples. *Food Chem.* **2023**, *402*, 134269. [CrossRef]
26. Dong, J.; Wen, L.; Zhao, D.; Yang, H.; Zhao, J.; Hu, Z.; Ma, Y.; Hou, C.; Huo, D. Flexible carbon fiber cloth supports decorated with cerium metal-organic frameworks and multi-walled carbon nanotubes for simultaneous on-site detection of Cd^{2+} and Pb^{2+} in food and water samples. *Food Chem.* **2023**, *418*, 135869. [CrossRef]
27. Huang, R.; Liao, D.; Chen, S.; Yu, J.; Jiang, X. A strategy for effective electrochemical detection of hydroquinone and catechol: Decoration of alkalization-intercalated Ti_3C_2 with MOF-derived N-doped porous carbon. *Sens. Actuators B Chem.* **2020**, *320*, 128386. [CrossRef]

28. Zhao, S.; Zhang, H.B.; Luo, J.Q.; Wang, Q.W.; Xu, B.; Hong, S.; Yu, Z.Z. Highly electrically conductive three-dimensional $Ti_3C_2T_x$ MXene/reduced graphene oxide hybrid aerogels with excellent electromagnetic interference shielding performances. *ACS Nano* **2018**, *12*, 11193–11202. [CrossRef]
29. Ma, Y.; Yue, Y.; Zhang, H.; Cheng, F.; Zhao, W.; Rao, J.; Luo, S.; Wang, J.; Jiang, X.; Liu, Z.; et al. 3D synergistical MXene/reduced graphene oxide aerogel for a piezoresistive sensor. *ACS Nano* **2018**, *12*, 3209–3216. [CrossRef]
30. Li, W.; Tong, J.; Li, G. Graphene oxide intercalated Alk-MXene adsorbents for efficient removal of Malachite green and Congo red from aqueous solutions. *Chemosphere* **2024**, *360*, 142376. [CrossRef]
31. Wang, S.; Cao, Z.; Zhang, Y.; Li, W. Study on the layering phenomenon of SiC porous layer fabricated by constant current electrochemical etching. *Nanotechnology* **2020**, *31*, 205702. [CrossRef]
32. Chahrour, K.M.; Hashim, M.R. Synthesis of SiC nanowires via controllable anodic etching time. *Appl. Phys. A* **2020**, *126*, 539. [CrossRef]
33. Naderi, N.; Moghaddam, M. Ultra-sensitive UV sensors based on porous silicon carbide thin films on silicon substrate. *Ceram. Int.* **2020**, *46*, 13821–13826. [CrossRef]
34. Meng, J.; Liu, X.; Niu, C.; Pang, Q.; Li, J.; Liu, F.; Liu, Z.; Mai, L. Advances in metal–organic framework coatings: Versatile synthesis and broad applications. *Chem. Soc. Rev.* **2020**, *49*, 3142–3186. [CrossRef]
35. Azar, M.H.; Ji, Z.; Jahanzamin, J.; Kitai, A. Fluorescent Silicon Carbide Quantum Dots. In *Silicon Carbide—From Materials Science to Nanotechnology and Microelectronics*; IntechOpen: London, UK, 2024. [CrossRef]
36. Prado, E.O.; Bolsi, P.C.; Sartori, H.C.; Pinheiro, J.R. An overview about Si, Superjunction, SiC and GaN power MOSFET technologies in power electronics applications. *Energies* **2022**, *15*, 5244. [CrossRef]
37. Qian, L.; Gu, Z.; Liu, M.; Deng, T.; Zhang, C.; Qian, J.; Huang, X.; Wang, C. Alkalized Ti_3C_2 MXene-engineered cost-effective pencil graphite electrode to develop high-performance electrochemical sensor for simultaneous detection of Cd^{2+} and Pb^{2+}. *Microchem. J.* **2025**, *213*, 113656. [CrossRef]
38. Zhang, Y.; Li, C.; Su, Y.; Mu, W.; Han, X. Simultaneous detection of trace Cd(II) and Pb(II) by differential pulse anodic stripping voltammetry using a bismuth oxycarbide/nafion electrode. *Inorg. Chem. Commun.* **2020**, *111*, 107672. [CrossRef]

Disclaimer/Publisher's Note: The statements, opinions and data contained in all publications are solely those of the individual author(s) and contributor(s) and not of MDPI and/or the editor(s). MDPI and/or the editor(s) disclaim responsibility for any injury to people or property resulting from any ideas, methods, instructions or products referred to in the content.